Effect of Hydrogen on the Structural and Phase State and Defect Structure of Titanium Alloy

Ekaterina Stepanova[a)], Yury Bordulev[b)], Victor Kudiiarov[c)], Roman Laptev[d)], Andrey Lider[e)] and Jiang Xinming[f)]

Tomsk Polytechnic University, 30 Lenina Avenue, Tomsk 634050 Russian Federation

[a)] corresponding author: enstepanova@tpu.ru
[b)] bordulev@gmail.com
[c)] victor31479@mail.ru
[d)] laptev.roman@gmail.com
[e)] lider@tpu.ru
[f)] 384390197@qq.com

Abstract. Effect of hydrogen on the structural and phase state of the fine- and ultrafine-grained structure of two-phase (alpha + beta) titanium Ti-6Al-4V alloy was investigated by the methods of electron microscopy and X-ray diffraction analysis. The defect structure of the fine- and ultrafine-grained samples before and after hydrogen treatment was studied by the implemented Positron lifetime technique. Hydrogenation is found to result in minor structural and phase changes both in fine- and ultrafine-grained samples. It is shown that defect structure of samples depends on the structural state and hydrogen presence.

INTRODUCTION

Two-phase (α + β-type) titanium alloys account for 90 % of commercial titanium alloys. The mechanical properties of the alloys essentially depend on their microstructure and phase composition. The formation of the ultrafine-grained (UFG) structure is known to be an effective method of improving the strength and operational characteristics of metal polycrystals at low homologous temperatures [1–4]. All most widely spread methods of the ultrafine-grained structure formation in metallic materials are based on Severe Plastic Deformation (SPD). The use of the SPD methods enables the sizes of the structural elements in the material to be decreased down to the nanolevel and, as a consequence, the strength characteristics to be increased by a factor of 1.5–2 [4–7]. At the same time, the rate of hydrogen absorption by metallic materials is known to be increased with decreasing grain sizes. Therefore, the prospects for the application of the UFG polycrystals as structural materials will largely be determined by the effect of hydrogen on the structural and phase state [5–8]. While penetrating into material, hydrogen produces a wide range of defects, such as vacancy clusters, and reacts with the existing ones, forming the so-called "defect-hydrogen" systems. In order to control the defect structure of beta-titanium, the positron annihilation techniques were used in this study. This method has shown to be effective in studies of hydrogenation effects on the defect structure of alpha-titanium [9–11]. Positron lifetime (PL) spectrometry allows identifying type, concentration and size of defects in material [12, 13].

On the basis of the above reasoning, we examine the effect of hydrogen on the structural and phase states of α + β-type titanium alloys in different structural states.

MATERIAL AND EXPERIMENTAL METHODS

As a material for the investigation, commercial two-phase α + β alloy Ti-6Al-4V (VT6 alloy grade) of the following composition in wt % was used: 6.6 Al + 4.9 V + 0.02 Zr + 0.033 Si + 0.18 Fe + 0.007 C + 0.17 O + 0.01 N + 0.002 H; the balance is Ti. Samples of the alloy in the initial fine-grained (FG) state were previously annealed at 1023 K for 1 hour.

Prospects of Fundamental Sciences Development (PFSD-2016)
AIP Conf. Proc. 1772, 030016-1–030016-6; doi: 10.1063/1.4964554
Published by AIP Publishing. 978-0-7354-1430-3/$30.00

The UFG state in the Ti-6Al-4V alloy was obtained by the method of three-dimensional pressing with the change of the deformation axis and gradual decrease of the deformation temperature at the Institute of Strength Physics and Materials Science SB RAS (Tomsk). First and second pressing to 60 % were performed at 873 K, third pressing to 75 % – at 853 K.

The alloy was hydrogenated to concentration of 0.05 % (hereinafter, the hydrogen concentration is indicated in weight percent) using the automated complex Gas Reaction Controller [15]. The temperature of hydrogenation was 823 K and hydrogen pressure was 2 atm. Hydrogenation mode has been selected on the basis of data obtained earlier [16], where it was shown that hour annealing at temperatures up to 923 K does not change the size of the grain-subgrain elements of the obtained UFG structure. The hydrogen concentration in the samples was measured by a RHEN 602 gas analyzer with ±0.0001% accuracy.

Thin foils were investigated using an EM-125K transmission electron microscope. The sizes of the structure elements were measured from micrographs by the secant method. The volume fractions and the lattice parameters of phases were determined with accuracies of ±1% and 0.0001 nm, respectively, using a Shimadzu XRD7000 diffractometer with Cu-K_α radiation source.

Spectrometer, that was implemented in this work for positron lifetime (PL) study was realized on a base of General Physics Department (Tomsk Polytechnic University). It has proven itself as an efficient tool for defect studies [9–11] of different materials. The scheme of this spectrometer is presented in Figure 1.

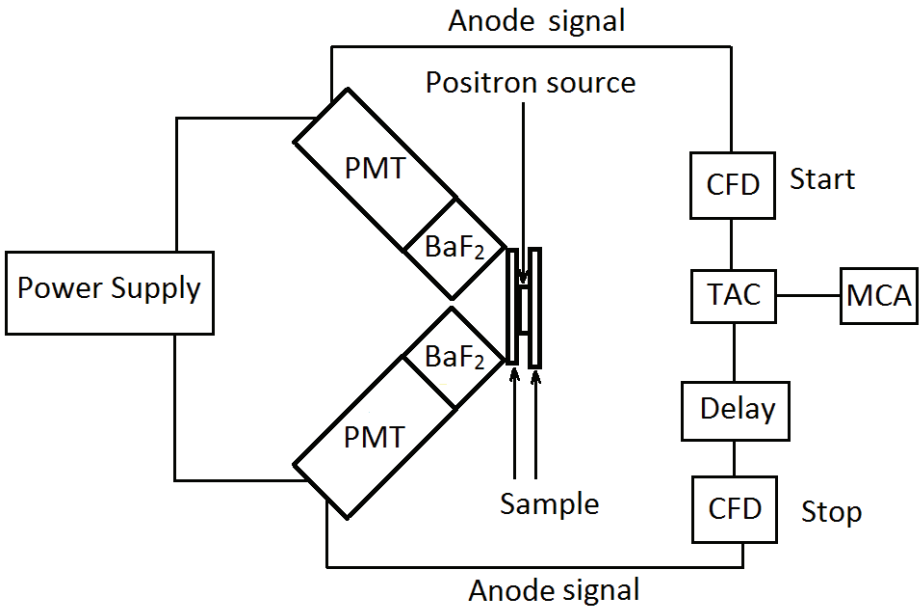

FIGURE 1. Scheme of positron lifetime spectrometer, implemented in this work.

The main difference of this spectrometer from the analogue setups is the alternative positron source on a base of 44Ti isotope. The maximum energy of positrons from this source equals 1.467 MeV, which allows study of defects on a higher depth, comparing to the conventional 22Na positron source. This spectrometer uses a conventional "fast-fast" circuit for positron lifetime determination by delayed coincidences technique. The principle of this technique is in measurement of time difference between two signals: registration of 1.157 MeV (Start signal) and 0.511 MeV γ-rays (Stop signal). This time difference corresponds to a positron lifetime. Spectrometer collects more than five millions of these lifetimes in a positron lifetime spectrum for each sample. The registration of γ-ray is performed by to scintillation detectors, based on photomultiplier tubes (PMT) Hamamatsu H3378-50 and BaF_2 scintillators (diameter of 30 mm and thickness of 25 mm). Anode signals from the detectors are then brought in to the inputs of differential constant fraction discriminators (CFD). Each of these two discriminators is tuned to pass only the Start or Stop signal, respectively. In such a manner, the outputs of these CFDs launch and stop the positron lifetime counting on a time to amplitude converter (TAC). The positron lifetime spectrum is then collected by multichannel analyzer. The time resolution of PL spectrometer and count rate are approximately 240 ps and 130 events/second, respectively. PL spectra were mathematically fitted by 2 Gaussians (resolution function) and several exponential components using special LT-10 software [17]. Each exponential component represents positron state in the material and is characterized by two values: positron lifetime in this state (τ), and intensity of this component (I). After positron source

substraction, experimental PL spectra were decomposed by two components. One of them corresponds to quasi-free positron state in the lattice of the material; another component corresponds to a positron state in a defect. The PL value, corresponding to positron, trapped in defect is increased, comparing to the PL in quasi-free state. This is due to the fact that the electron density in defect is usually lower than the electron density in perfect crystal.

Test specimens shaped as plate with sizes 10 x 10 x 1 mm were cut from billets by the electrospark method. Before testing, the specimen surfaces were subjected to mechanical grinding and electrolytic polishing.

EXPERIMENTAL RESULTS AND ITS DISCUSSION

In the initial state the Ti-6Al-4V alloy has inhomogeneous structure consisting of α single-phase and α + β two-phase regions (Figure 2). The single-phase regions 10–40 μm in size, as a rule, are surrounded by the two-phase regions. According to X-ray diffraction data, in the volume fraction of the β phase is 3%. Furthermore, the texture with a Dollas-March coefficient of 0.6741 is observed in the alloy in the [002] direction.

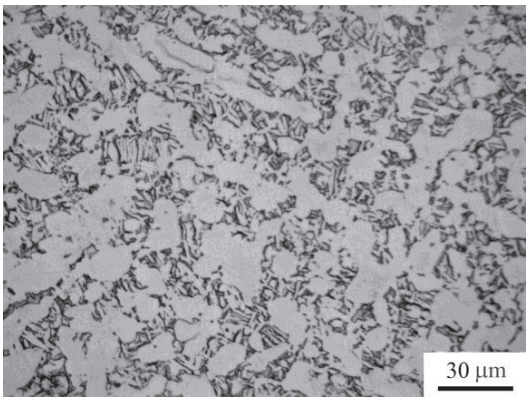

FIGURE 2. Microstructure of the Ti-6Al-4V alloy in the initial FG state

TABLE 1. Phase composition and lattice parameters of the Ti-6Al-4V alloy in different states

Condition	Volume fraction of the α phase, %	Volume fraction of the β phase, %	Phase lattice parameters		
			a_α, nm	c_α, nm	a_β, nm
FG	97	3	0.2926	0.4683	0.3152
UFG	95	5	0.2921	0.4655	0.3183
FG+0.05H	98	2	0.2878	0.4689	0.3156
UFG+0.05H	93	7	0.2922	0.4660	0.3253

The typical structure of the examined UFG Ti-6Al-4V alloy after deformation with the change of the deformation axis is shown in Fig. 3. It is evident that an entangled deformational contrast is observed and some structure elements are poorly distinguished on the bright-field image of the structure. Individual grain and subgrains are visible on the dark-field image (Fig. 3, b). The size distribution of grain-subgrain structure elements of the obtained structure is subjected to the normal-logarithmic law (on the histogram $\Delta N/N_0$ is a fraction of structural elements with the given grain size to the total amount of elements) (Fig. 3, c). The average size of the structure elements was 0.29 μm. Quite a number of reflections uniformly spaced on a circle are observable in the microdiffraction image of such a structure recorded from the area of 1.4 μm^2 (Fig. 3, a). Thus, many reflections have azimuthal blurring. Such a type of microdiffraction is typical for ultrafine-grained materials with high misorientations between the elements of grain/subgrain structure, nonequilibrium grain boundaries, and internal fields of compressive stresses.

By the methods of X-ray structural analysis it was established that by analogy with the fine-grained state only α and β phases are registered in the UFG Ti-6Al-4V alloy. The volume fraction of the β phase calculated from the X-ray diffraction pattern was about 5 vol. %. In addition, as the result of the UFG structure forming the redistribution of the reflection intensities (101) and (002) of the α phase occurs. This indicates that during pressing with the change of deformation axis texture in the [002] direction disappears.

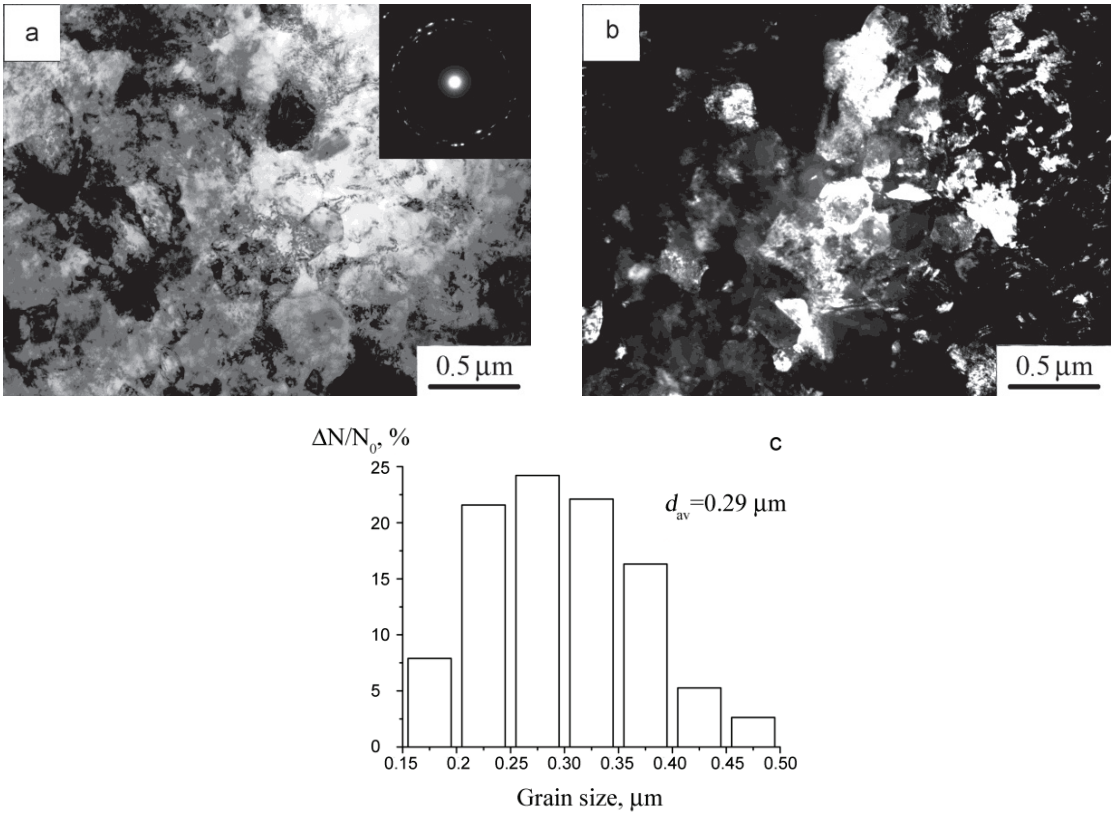

FIGURE 3. Electron microscope image of structure (a, b) and a histogram of grain size distribution (c) for the ultrafine-grained Ti-6Al-4V alloy: (a) bright-field image and microdiffraction pattern; (b) dark-field image

Fig. 4 demonstrates the curves of the hydrogen sorption in the samples of the Ti-6Al-4V alloy in FG (1) and UFG (2) states on the time of hydrogenation. It is seen that the rate of hydrogen sorption by the UFG alloy is substantially (~16 times) higher than for the FG alloy samples. Hydrogen concentration measurements made by RHEN602 after hydrogenation up to the concentration of 0.05 % have shown that the real concentrations are 0.0215 and 0.035 % for FG and UFG samples, respectively.

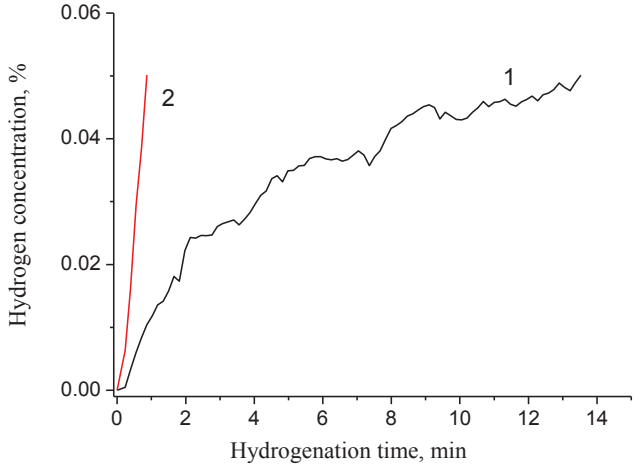

FIGURE 4. Curves of hydrogen sorption for titanium Ti-6Al-4V alloy in fine-grained (1) and ultrafine-grained (2) states

Electron microscopic studies have shown that hydrogenation insignificantly changes the structural state of the titanium alloy samples in both states. At the same time, according to X-ray structural analysis (Table 1)

hydrogenation of the FG alloy to the concentration of 0.05 % results in increase in the lattice parameter of the β phase. At the same time, the texture in the [002] direction in the alloy retains. Hydrogenation of the UFG alloy to the concentration of 0.05 % leads to an increase in the volume fraction of the β phase. The lattice parameter of the β phase is considerably larger than that in an initial state because of hydrogenation.

Results of PL study of the titanium Ti-6Al-4V alloy in the UFG and FG states before and after hydrogenation are presented in the Table 2.

Table 2. Positron annihilation characteristics of the investigated samples of Ti-6Al-4V alloy

Sample	τ_1, ps	τ_2, ps	I_2
FG	147	-	-
UFG	120	178	71
FG + 0.05 % of hydrogen	144	-	-
UFG + 0.05 % of hydrogen	80	170	84

PL spectrum analysis of annealed sample revealed appearance only one component with the lifetime of 147 ps. This value agrees with the literature data [18, 19] for bulk titanium. After the process of hydrogen saturation of FG sample the lifetime of this component become lower. This means increase of electron density in the material. One of the reasons, which can lead to such increase, can be the dissolution of hydrogen in crystal lattice.

As it can be seen from the Table 1, spectrum for the UFG sample of titanium alloy in the initial state shows appearance of the defect component with lifetime of 178 ps. This value is equal to the lifetime of positron, trapped at dislocation or low-angle boundaries [20]. These defects were formed during the severe plastic deformation, and their contribution in the spectrum is rather high (71 %). The lifetime of first component (τ_1) decreases, which is a regular change according to the simple trapping model [17]. After hydrogen saturation, the lifetime of defect component (τ_1) slightly decreases, while its intensity increases till the value of 84 %. This means, that hydrogen reduces open volume of defects in the material, but at the same time increase the concentration of these defects. One of the explanations of such a process can be the idea that hydrogen "fills" the open volume of the existing grain boundaries, while increasing the concentration of grain boundaries in the material.

CONCLUSION

Thus, SPD by pressing with the change of deformation axis and gradual temperature decrease at temperature range of 873–853 K leads to formation of nonequilibrium ultrafine-grained structure with an average size of grain-subgrain structure elements of 0.29 μm in titanium Ti-6Al-4V alloy.

The rate of hydrogen sorption by the UFG alloy is substantially (~16 times) higher than for the FG alloy samples.

In the FG Ti-6Al-4V material after hydrogen saturation to the concentration of 0.05 % from the gas media, the lattice expansion of the β phase is observed. There are no evidences of defects in the material at this concentration level.

In the UFG Ti-6Al-4V material the dominant defects are dislocations and grain boundaries. After hydrogen saturation till the concentration of 0.05 % from the gas media, the open volume of grain boundaries decreases while concentration of such a defects increases.

ACKNOWLEDGMENTS

This work was funded within the framework of realisation of Strategic Programme on National Research Tomsk Polytechnic University Competitiveness Enhancement in the Group of Top Level World Research and Academic Institutions.

REFERENCES

1. D. G. Morris, *Mechanical behavior of nanostructured materials* (Trans. Tech. Publication ltd, Switzerland, 1998), p. 85.
2. E. N. Stepanova, G. P. Grabovetskaya, O. V. Zabudchenko, and I. P. Mishin, Rus. Phys. J. **54**(6), 690–696 (2011).
3. M. A. Meyers, A. Mishra, and D. J. Benson, Progr. Mater. Sci. **51**, 427–556 (2006).

4. R. Z. Valiev, Y. Estrin, Z. Horita, T. G. Langdon, M. J. Zehetbauer, and Y. T. Zhu, Mater. Res. Lett. **4**(1), 1–21 (2016).
5. G. P. Grabovetskaya, E. N. Stepanova, I. V. Ratochka, E. V. Naidenkin, and O. N. Lykova, Inorganic Materials: Applied Research. **4**(2), 92–97 (2013).
6. G. P. Grabovetskaya, E. N. Stepanova, I. V. Ratochka, I. P. Mishin, and O. V. Zabudchenko, Mater. Sci. Forum. **838-839**, 344–349 (2016).
7. G. Salishchev, R. Galeev, S. Malysheva, S. Zherebtsov, S. Mironov, O. Valiakhmetov, and E. Ivanisenko, Metal Sci. Heat Treat. **608**, 63–69 (2006).
8. E. N. Stepanova, G. P. Grabovetskaya, and I. P. Mishin, J. Alloys Compd. **645**, S271–S274 (2015).
9. Y. Bordulev, R. Laptev, V. Kudiyarov, and A. Lider, Adv. Mater. Res. **880**, 93–100 (2014).
10. R. S. Laptev, Y. S. Bordulev, V. N. Kudiyarov, A. M. Lider, and G.V. Garanin, Adv. Mater. Res. **880**, 134–140 (2014).
11. A. Lider, O. Khusaeva, Y. Bordulev, R. Laptev, and V. Kudiyarov, Adv. Mater. Res. **1085**, 328–334 (2015).
12. V. Grafutin, and E. Prokopev, Physics-Uspekhi. **45**(1), 59–74 (2002).
13. R. Laptev, A. Lider, Y. Bordulev, V. Kudiiarov, and G. Garanin, J. Alloys Compd. **645**, S193–S195 (2015).
14. R. Krause-Rehberg, and H. S. Leipner, *Positron Annihilation in Semiconductors: Defect Studies* (Springer-Verlag Berlin and Heidelberg, Berlin, 1999), p. 378.
15. V. Kudiiarov, L. Gulidova, N. Pushilina, and A. Lider, Adv. Mater. Res. **740**, 690–693 (2013).
16. I. P. Mishin, G. P. Grabovetskaya, O. V. Zabudchenko, and E. N. Stepanova, Rus. Phys. J. **57**(4), 423–428 (2014).
17. D. Giebel, and J. Kansy, Physics Procedia. **35**, 122–127 (2012).
18. J. M. C. Robles, E. Ogando, F. Plazaola, J. Physics. Condens. Matter. **19**, 176222 (2007).
19. J. M. C. Robles, E. Ogando, F. Plazaola, J. Phys. Conf. Ser. **265**, 012006 (2011).
20. N. Nancheva, K. Saarinen, and G. Popov, Physica Status Solidi (a). **95**(2), 531–536 (1986).